Experimental Investigation on Rapid Filling of a Large-Scale Pipeline

Qingzhi Hou[1]; Arris S. Tijsseling[2]; Janek Laanearu[3]; Ivar Annus[4]; Tiit Koppel[5]; Anton Bergant[6]; Sašo Vučković[7]; Alexander Anderson[8]; and Jos M. C. van 't Westende[9]

Abstract: This study presents the results from detailed experiments of the two-phase pressurized flow behavior during the rapid filling of a large-scale pipeline. The physical scale of this experiment is close to the practical situation in many industrial plants. Pressure transducers, water-level meters, thermometers, void fraction meters, and flow meters were used to measure the two-phase unsteady flow dynamics. The main focus is on the water–air interface evolution during filling and the overall behavior of the lengthening water column. It is observed that the leading liquid front does not entirely fill the pipe cross section; flow stratification and mixing occurs. Although flow regime transition is a rather complex phenomenon, certain features of the observed transition pattern are explained qualitatively and quantitatively. The water flow during the entire filling behaves as a rigid column as the open empty pipe in front of the water column provides sufficient room for the water column to occupy without invoking air compressibility effects. As a preliminary evaluation of how these large-scale experiments can feed into improving mathematical modeling of rapid pipe filling, a comparison with a typical one-dimensional rigid-column model is made. **DOI: 10.1061/(ASCE)HY.1943-7900.0000914.**

Author keywords: Experimentation; Large-scale pipeline; Unsteady flow; Two-phase flow; Air–water interface; Flow-regime transition.

Introduction

Rapid pipe filling occurs in various hydraulic applications, such as water-distribution networks, storm-water and sewage systems, fire-fighting systems, oil transport, and pipeline cleaning and priming. While the water column is driven by a high head, air is expelled by the advancing water column. If the generated air flow is not blocked by obstacles, such as gates, valves or orifices, the water column grows with little adverse pressure and may attain a high velocity. When the advancing column is suddenly stopped (fully or partially), severe pressure changes will occur in the system (e.g., Guo and Song 1990; De Martino et al. 2008; Bergant et al. 2010, 2011; Martin and Lee 2012).

[1]Lecturer, State Key Laboratory of Hydraulic Engineering Simulation and Safety; and School of Computer Science and Technology, Tianjin Univ., Tianjin 300072, China (corresponding author). E-mail: qhou@tju.edu.cn

[2]Assistant Professor, Dept. of Mathematics and Computer Science, Eindhoven Univ. of Technology, P.O. Box 513, 5600 MB, Eindhoven, Netherlands.

[3]Associate Professor, Dept. of Mechanics, Tallinn Univ. of Technology, Ehitajate tee 5, 19086 Tallinn, Estonia.

[4]Teaching Assistant, Dept. of Mechanics, Tallinn Univ. of Technology, Ehitajate tee 5, 19086 Tallinn, Estonia.

[5]Professor, Dept. of Mechanics, Tallinn Univ. of Technology, Ehitajate tee 5, 19086 Tallinn, Estonia.

[6]Head, R&D Dept., Litostroj Power d.o.o., Litostrojska 50, Ljubljana 1000, Slovenia.

[7]Sales Manager, Sales Dept., Litostroj Power d.o.o., Litostrojska 50, Ljubljana 1000, Slovenia.

[8]Senior Lecturer, School of Mechanical and Systems Engineering, Newcastle Univ., Newcastle upon Tyne NE1 7RU, U.K.

[9]Senior Engineer, TNO, P.O. Box 155, 2600 AD, Delft, Netherlands.

Note. This manuscript was submitted on June 22, 2013; approved on April 23, 2014; published online on July 9, 2014. Discussion period open until December 9, 2014; separate discussions must be submitted for individual papers. This paper is part of the ***Journal of Hydraulic Engineering***, © ASCE, ISSN 0733-9429/04014053(14)/$25.00.

Rapid filling processes in single pipes have been studied experimentally before. Nydal and Andreussi (1991) investigated the air entrainment in a water column advancing over a liquid film in a nearly horizontal pipe that was 17 m long and 50 mm in diameter. It was found that air entrainment occurred only when the relative velocity between the advancing front and the liquid layer was greater than a threshold $2D/W_i$ (W_i = interfacial width). When there was no initial liquid film in the pipe, air entrainment did not occur. Liou and Hunt (1996) investigated the rapid filling of a 7-m-long pipe with a diameter of 23 mm. A high but short-lived peak velocity occurred after which the velocity slowly decreased to its steady state value. To check the validity of the planar front assumption in the rigid-column model of Liou and Hunt (1996), Vasconcelos et al. (2005) studied the filling process of a 14-m-long and 94-mm-diameter pipe for three different driving heads. It was observed that the advancing water column did not entirely fill the pipe cross section, and a stratified flow was observed behind the leading front.

In the context of pipe filling, the usual focus was on the physical factors affecting the peak transient pressure, such as the location and size of entrapped air pocket(s), the water column length, the driving pressure head, and the size of the end orifice (Martin 1976; Ocasio 1976; Cabrera et al. 1992, 1997; Izquierdo et al. 1999; Lee and Martin 1999; Zhou 2000; Liu and Suo 2004; Lee 2005; De Martino et al. 2008; Zhou et al. 2011; Martin and Lee 2012; Zhou et al. 2013a, b). Ocasio (1976) carried out experiments with entrapped air pockets at a dead end and demonstrated that the presence of entrapped air could result in destructive pressure surges. This is consistent with the conclusions drawn by Martin (1976). Lee and Martin (1999), Zhou (2000), and Lee (2005) investigated the effect of relatively large entrapped air pockets (initial void fractions between 6 and 45%) in horizontal pipelines with dead ends. They found that the maximum peak pressure of the air pocket increased with the decrease of its initial size. As a complementary work, Zhou et al. (2011) presented experimental measurements in an undulated pipeline with small initial void fraction

(from 0 to 10%). They found that the maximum peak pressure of the air pocket first increased and then decreased with decreasing void fraction. For the filling of pipelines with undulating profile, multiple air pockets and an open end, the rapid compression of the entrapped air may cause huge pressures (Cabrera et al. 1997; Izquierdo et al. 1999; Zhou et al. 2013a). When two air pockets are entrapped, the case with similar sizes was the most complicated and dangerous one (Zhou et al. 2013a). To investigate the behavior of the air entrapped in a drainage system, Yamamoto et al. (2000) presented an experimental study that involved the use of a horizontal pipe with a length of 122 m and a diameter of 200 mm. The entrapped air increased both the pressure rise time and the pressure peak. Zhou et al. (2002) investigated the rapid filling of a horizontal pipe with an end orifice that was partially full with water. The pipe length was 9 m and the diameter was 35 mm. The focus was on pressure surges influenced by the initial water depth, the orifice size, and the driving head. It was demonstrated that air trapped in a rapidly filled pipe can induce high-pressure surges, especially when air leakage occurred at the orifice. Three types of pressure oscillation patterns were observed, depending on the size of the orifice. Recently, to ascertain the effect of entrapped air and orifice size on pipeline transients, a similar experimental test program was reported by Martin and Lee (2012) with results similar to those in Yamamoto et al. (2000).

To study the transition from free surface to pressurized flow in sewers during storm events, Trajkovic et al. (1999) conducted experiments in a test rig consisting of a circular pipe with downward slope and gates at the upstream and downstream ends. The overall pipe length was approximately 10 m and the pipe diameter was 100 mm. It was found that the supercritical free-surface flow at the upstream end (under proper ventilation) always induced a hydraulic jump. Recently, inspired by the work of Trajkovic et al. (1999), a similar experimental investigation was conducted by Trindade and Vasconcelos (2013) with modifications that limited the ventilation conditions. For the study of flow-regime transition and the interaction between air and water phases, Vasconcelos (2005) and Vasconcelos and Wright (2005) conducted rapid filling experiments of a poorly ventilated storm-water tunnel. The pipe was initially empty or partially filled with water. It was found that the air near the pipe crown could pressurize and influence the flow dynamics. The surge intensity was maximized when a hydraulic bore propagated toward the surge riser [also observed by Nydal and Andreussi (1991)], and it increased with the pressure head behind the pressurization front. In this respect, the current paper provides useful experimental information that complements the previous studies on pipeline filling.

These previous studies show that for the filling of a small-scale horizontal system with relatively high driving head, the deformation of the water front has an insignificant effect on the overall hydrodynamics of the lengthening water column (Hou et al. 2012b). Thus, a planar water–air interface is often assumed. However, it is not clear in advance whether this assumption is applicable to large-scale pipelines. This issue is of high importance to understand the development of air pockets and gravity currents during the filling process. The present experimental investigation aims at a better understanding of the evolution of the moving interfaces, the pressure distribution, and the flow rates. To assist in interpreting the experimental results, they are compared with predictions from a one-dimensional model that has the conventional planar water–air interface assumption. This paper complements the experimental work done in the same Deltares pipeline apparatus on the emptying of it by different upstream compressed-air pressures and with different outflow restriction conditions (Laanearu et al. 2012).

Experimental Apparatus

The experimental apparatus consisted of a water tank, an air tank, steel supply pipelines (for water and air), a polyvinyl chloride (PVC) inlet pipe, a pipe bridge, a horizontal long PVC pipeline (the test section), an outlet steel pipeline, and a basement reservoir. Detailed information is provided subsequently, and part of it can be found in Lubbers (2007), Laanearu et al. (2009, 2012), Laanearu and van 't Westende (2010), and Hou (2012). The downstream end of the PVC pipe bridge was defined as the origin of the coordinate system. It is the starting point of the test section. The x-coordinate follows the central axis of the pipeline, the y-coordinate is not used in this study, and the z-coordinate is the vertical elevation. Coordinates of measuring instruments and other important components are shown in Fig. 1.

A water tank with a constant 25-m head relative to the center line of the inlet ($x = -34.6$ m) was used to supply water in the filling experiment reported in this paper, and an air tank with a 70-m^3 volume was used to supply air in the emptying experiment (Laanearu et al. 2012). The horizontal inlet steel pipe from the tank to the vertical leg was 2.6-m long. The vertical leg of the Y-junction was 3.6-m long. The steel pipe, from the Y-junction ($x = -27.2$ m) to the upstream steel–PVC connection ($x = -14$ m) was 13.2-m long. The air supply steel pipe, from the check valve ($x = -43.1$ m) to the Y-junction, was 15.9-m long. The inner diameter of the steel pipes was 206 mm, with a wall thickness of 5.9 mm. The PVC pipe was 275.2-m long and its outer diameter was 250 mm with an average wall thickness of 7.3 mm. It consisted of two parts. The first part consisted of a 7.5-m-long PVC inlet pipe and a 6.5-m-long pipe bridge. It led from the upstream steel–PVC connection ($x = -14$ m) to the chosen starting point of the test section ($x = 0$). With the aid of a piezometer tube, the bridge was used to set up the initial water column. The second part was the horizontal PVC pipe of length 261.2 m (from $x = 0$ to the downstream PVC–steel connection). Most of the measurements took place in this section. The outlet steel pipe led from the downstream end of the PVC pipe to the basement reservoir. It contained two segments of different diameters connected by a reducer. The reducer had a length of 0.3 m and was located 0.3 m upstream of the outlet flow meter. The first segment was 8.8-m long and the inner diameter was 260.4 mm with a wall thickness of 6.3 mm. The second segment was 2-m long and the inner diameter was 206 mm with a wall thickness of 5.9 mm. The pipeline had downward turns at $x = -27.2$ m and $x = 267.0$ m, and an upward turn at $x = -31.6$ m. The elevation information is shown in Fig. 1. The downward leg beyond $x = 267.0$ m formed a siphon after the water front arrived at the last elbow.

Pipe Supports and Connections

To suppress pipe motion and associated fluid–structure interaction (FSI) effects (e.g., Bergant et al. 2010, 2011; Keramat et al. 2012; Tijsseling 1996; Wiggert and Tijsseling 2001), it was attempted to structurally restrain the pipe system as much as possible. The PVC pipeline was fixed to the concrete floor by metal anchors and supported with wooden blocks to reduce sagging. The pipe bridge—elevated 1.3 m above the main pipeline axis—was supported by a tube frame. As it appeared hard to fix the most downstream elbow ($x = 267.0$ m), a heavy mass (approximately 1 t) was attached with a rope at this point to reduce the elbow's vertical movement. The PVC pipeline segments were connected by sleeves. Wherever the PVC pipe needed to change direction, a large-radius bend ($R = 5D_{\mathrm{PVC}}$) was used. There were four 90° bends in the test section and a long bend at the 180° turning point (Fig. 1).

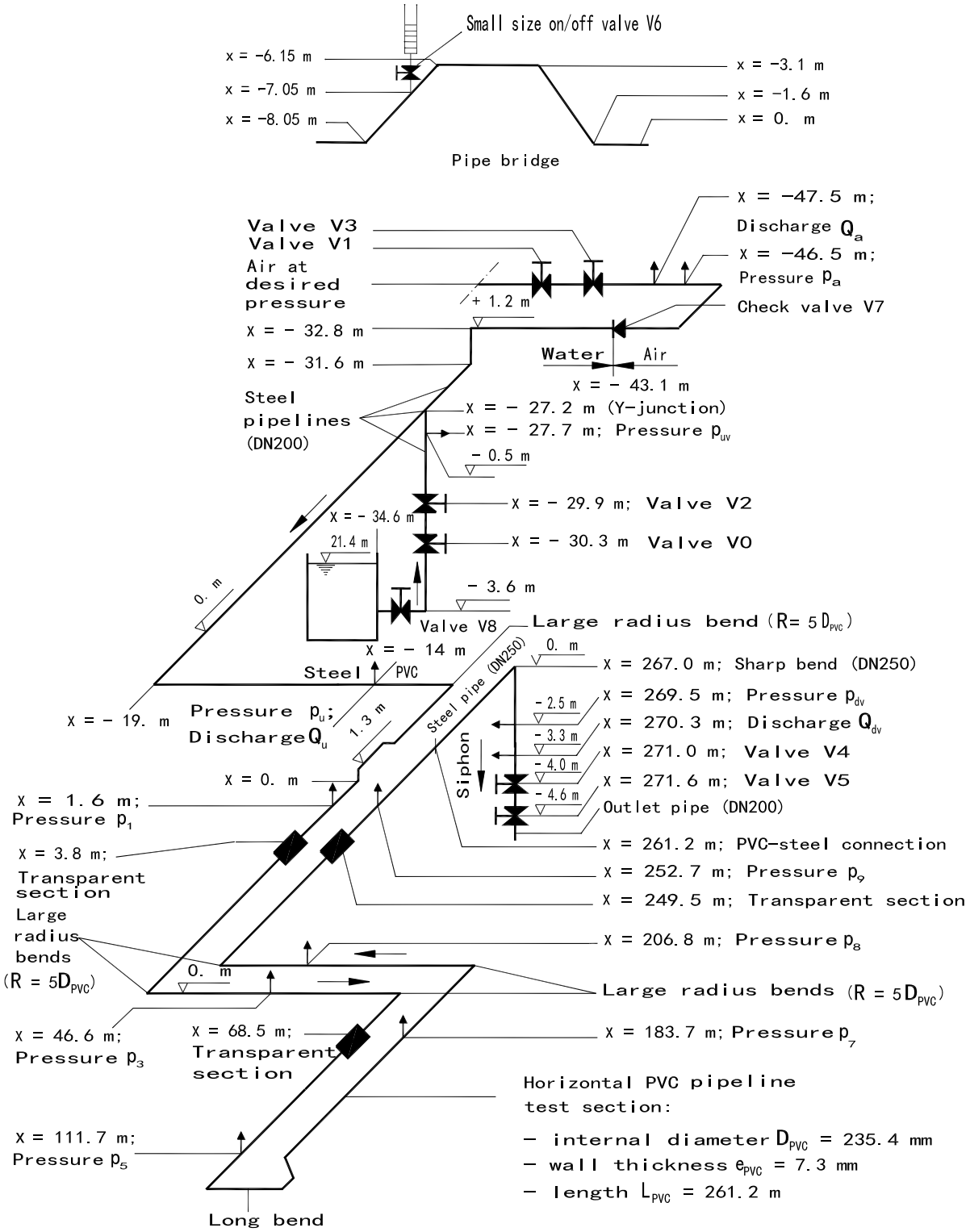

Fig. 1. System dimensions and coordinates of the measuring instruments (adapted from Bergant et al. 2011, with permission)

There were nine valves in the system as indicated in Fig. 1. Several small air venting valves are not shown; most of the venting valves were located upstream of the pipe bridge. All of them were closed in the filling process, which is different from the upstream ventilation condition used in the filling tests by Trajkovic et al. (1999) (full ventilation) and Trindade and Vasconcelos (2013) (limited ventilation). The check valve (V7 at $x = -43.1$ m) was used to prevent entrance of water into the air system. The water inlet valve (V8 at $x = -34.6$ m) connected to the water tank remained open during all experiments. The other seven valves labeled V0 to V6 were actively operated manually or automatically (Fig. 1). Three of them (V0, V2, and V6) were used in the filling tests. The upstream service valve V0 (DN200) was operated manually to supply water. The automatic control valve V2 (DN150) was used for flow regulation. The small-size on/off valve V6 in the transparent stand tube mounted at the upstream leg of the pipe bridge (Fig. 1) was open when monitoring the initial position of the front of a nearly static water column. All of the water valves used in

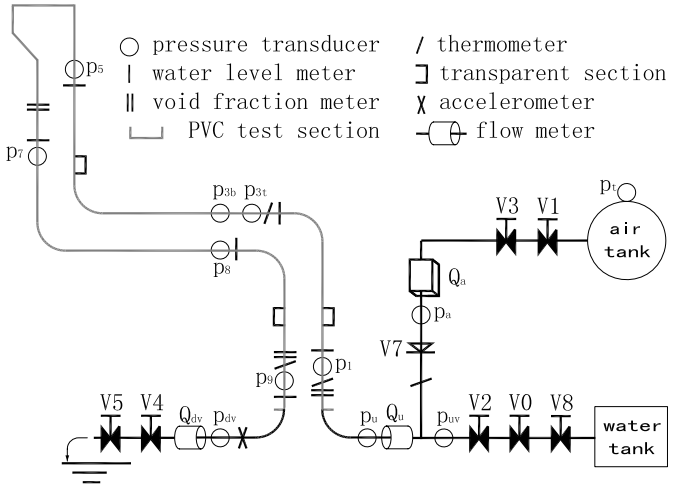

Fig. 2. Layout of measuring instruments in the pipeline apparatus

the system were butterfly valves and the check valve (V7) was a cage valve.

Instruments and Data Acquisition

Instruments. A maximum of 29 instruments were installed along the whole system as sketched in Fig. 2. There were 12 pressure transducers, 6 water level meters, 4 thermometers, 3 void fraction meters, 3 flow meters, and 1 accelerometer. The coordinates of the pressure transducers and flow meters are shown in Fig. 1. The coordinates of the other measuring instruments can be found in Hou et al. (2012a), where the type, output range, position (within the pipe cross section), and other relevant information are provided. The three transparent sections had lengths of 0.7 m with 0.5-m-long viewing windows. A Sony DXC-990P camera was set up at the first and last sections (Fig. 2) and recorded the water–air interfaces and the air–water mixing process. The nine measuring sections were numbered (indicated by the subscripts of variables in Figs. 1 and 2) in sequence from upstream to downstream.

Uncertainties. According to nominal values provided by the manufacturers, the estimated uncertainty under steady-state conditions was ±1.0% (percent of reading) in the flow-rate measurements, ±0.1% (percent of reading) in the pressure measurements, and ±0.8°C in the temperature measurements. A conductivity probe instrument uncertainty is typically ±1 mm, but in this application it will be significantly greater because of both its transient response time and also the observed significant turbulent disturbance of the water–air interface in the wave-front region. Transient calibration comparisons with camera images suggest an uncertainty as high as ±15 mm, partly because of water film formation on the walls of the transparent section, which reduced the visibility. All pressure transducers were of the strain-gauge type with a natural frequency of 10 kHz. They were all installed flush-mounted at the pipe sides, except for p_3. Apart from the uncertainties in the measuring devices, there were also uncertainties in the filling process itself.

- The response times of the measuring instruments were different. For example, for the pressure transducer and the flow meter located at the same place, the response of the pressure transducer was normally 1 s earlier than the response of the flow meter. The instant of the first response of the flow meter at $x = -14$ m was taken as time $t = 0$.
- The PVC pipeline was intended to be entirely empty before each pipe filling run. However, it was found that some water remained between Sections 3 ($x = 46.4$ m) and 8 ($x = 206.8$ m) after a filling and subsequent emptying run. The amount of uncleared water varied per test. With valve V4 fully open and using high-pressure air (more than 1 bar) to drain the pipe, the depth of remaining water was approximately 30 mm on average and up to 60 mm when air at low-pressure (less than 1 bar) was used. The experimental results examined in this sutdy were obtained after draining with high-pressure air. For the average depth of 30 mm (between sections 3 and 8), the volume of the remaining water was 0.52 m^3, which is equivalent to the volume of 12 m of the PVC pipe.
- Before each pipe filling run, the air entrapped in the steel pipe between the Y-junction ($x = -27.2$ m) and the check valve ($x = -43.1$ m) was not released. It is not clear what its effect is on the filling process in general and air entrainment in particular.

Data acquisition. Deltares's 32-channel data acquisition system was used for synchronized recording of flow rate (inflow Q_u, outflow Q_{dv}, air flow Q_a), pressure (p_1, p_{3t}, p_{3b}, p_5, p_7, p_8, p_9, p_u, p_{uv}, p_{dv}, p_a, p_t), temperature (T1, T3, T9, T_a), water level (WL1, WL3, WL5, WL7, WL8, WL9), and void fraction (VF1, VF3, VF9) (Fig. 2). Video camera and accelerometer recordings were not electronically synchronized with the data acquisition recordings. The camera images were highly useful to get direct visual information on the two-phase flow structure developing in the pipe. A sampling rate of 100 Hz was used to record discharge, gauge pressure, water level, void fraction, and temperature.

Test Procedure

All pipe-filling experiments were carried out with the downstream valves V4 and V5 fully open and a constant driving head of 25 m (at $x = -34.6$ m, $z = -3.6$). Air at atmospheric pressure and some stagnant water is initially present in the system. First, the upstream valve V0 was opened manually. Then the automatic valve V2 was opened from 0 to 15% until the height of the water in the pipe bridge reached a vertical level of 0.4 m (0.04 barg reading from pressure transducer p_u at $x = -14$ m as shown in Fig. 1). After closing valve V2, the water level at $x = -6.5$ m (which is at the upstream leg of the bridge) was allowed to gradually reach the level of 1.0 m (visually observed from the piezometer tube) because of a small leakage of valve V2. When this level was reached, the upstream pipe was full and the top of the bridge was empty. Filling then started by closing the small valve V6 on the piezometer tube and by fully opening valve V2 at the same time. The filling was rapid, within one minute time. After that, a steady state was reached, i.e., the inlet and outlet flow discharges were equal and constant, and the outlet control valve V4 was closed slowly by hand from 0 to 75° (labeled on a panel) to avoid any pressure surges. After the gradual closure of valves V5 and V2, the filling process was completed.

Experimental Results

Steady-State Friction and Resistance

Before the rapid pipe-filling experiments, full-pipe steady-flow measurements were carried out to determine the system's head loss characteristics. At a steady-state flow velocity of 4 m/s, the hydraulic grade line for the PVC pipe is shown in Fig. 3. The straight hydraulic grade line for $x > 0$ confirms that the pipe test section was long enough to neglect the minor losses resulting from the bends (necessary to accommodate the pipe length within the laboratory). Laanearu et al. (2012) have shown that the steady-state friction factor of the test pipe was $f = 0.0136$ and the 180° turn loss-coefficient was $K_{lb} = 0.06$. The friction head loss over the $L = 275.2$ m PVC pipe was $h_f = 13$ m; in comparison the local

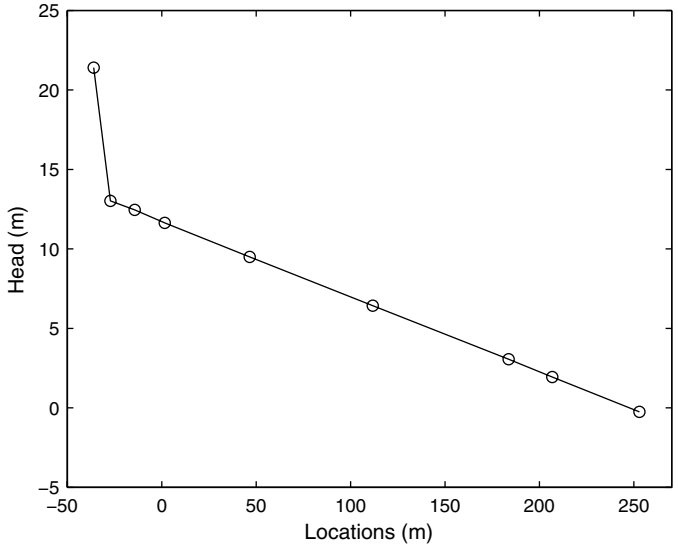

Fig. 3. Steady-state hydraulic grade line

head loss $h_{lb} = 0.05$ m resulting from the 180° turn was negligible. The large head loss in the upstream part of the pipeline from $x = -34.6$ m to $x = -27.7$ m was primarily because of the resistance of the valves V0, V2, and V8.

Flow Rates

The upstream and downstream flow rates measured during filling are shown in Fig. 4, in which good repeatability is exhibited by the three representative runs. The arrival time of the water column at the downstream flow meter ($x = 270.3$ m) is 54 ± 0.8 s. The area covered by the inflow rate curve and the time-axis between $t = 0$ and $t = 54$ s is the amount of water that has been fed into the pipeline. The estimated value is 11,150 L. It is less than the empty pipe volume $\forall = AL = \pi D_{\text{PVC}}^2/4 \times (270.3 + 6.5) \times 10^3 = 12{,}000$ L (water column front starts at $x = -6.5$ m), from which the volume of water present before filling (approximately 500 L) must be subtracted. The volume discrepancy of 350 L is equivalent to the volume of 8-m length of PVC pipe. This implies that when the water column arrives at the downstream flow meter, not all air is expelled out of the system. This matter is examined further in the next section.

Now the focus shifts to the measurements by the upstream flow meter ($x = -14$ m). As shown in Fig. 4, the flow rate first rises to its maximum value of 270 ± 3 L/s in approximately 4 s. Then it decreases rapidly from 270 to 250 L/s in 2-s time. After that, the flow gradually decelerates until a steady state of fully filled pipe flow is reached with short-living water hammer as a result of the slug effect. The inflow velocity V—determined from the averaged flow rate of 9 runs—is shown in Fig. 5 by the solid line. The trend of the curve is the same as that in the small-scale experiment of Liou and Hunt (1996), although the filling time is over 11 times longer in this study (approximately 57 s versus 5 s), primarily because of the longer pipe length. The measured maximum velocities are higher (approximately 6.2 m/s versus 1.6 m/s), primarily because of the higher driving head in the present experimental setup.

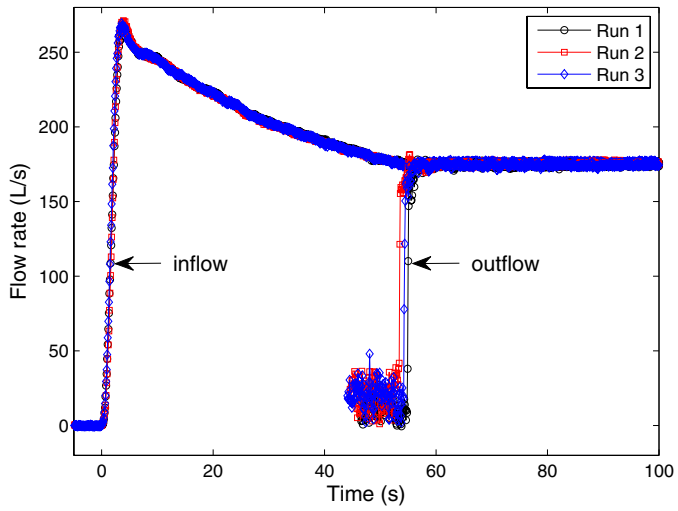

Fig. 4. Measured inflow and outflow rates in three typical pipe filling runs

Water–Air Interfaces

Because the initial static water front (water–air interface) splits into two water fronts during the filling process, the sketch in Fig. 6 is introduced for the sake of clarity. To determine the water front velocities V_1 (leading front) and V_2 (secondary front) [Fig. 6(c)], the measuring method of Liou and Hunt (1996) is used. Two different groups of instruments are used for the front timing sections. The first group consists of the six water-level meters (WL1, WL3, WL5, WL7, WL8, and WL9) located at $x = 1.7$, 46.4, 111.7, 183.7, 206.8, and 252.9 m, respectively. The second group consists of the six pressure transducers (p_1, p_{3b}, p_5, p_7, p_8, and p_9) located at $x = 1.6$, 46.6, 111.7, 183.7, 206.8, and 252.8 m, respectively. Except for pressure transducer p_{3b}, which is located at the pipe bottom, the other five transducers are in a horizontal plane with the pipeline axis. The water-level meters are in a vertical plane with the pipeline axis. The arrival times of the advancing water fronts at the timing sections are captured by the two groups of instruments. The average speeds of the fronts are then computed as the distances between the timing sections divided by the travel times.

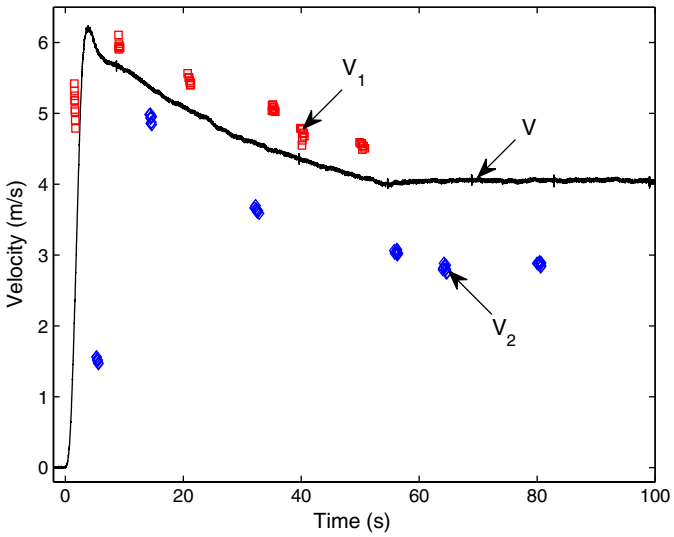

Fig. 5. Velocity history of the inflow and the water fronts in the filling experiments; solid line, adapted from upstream flow measurements; symbols, indirect measurements (squares, V_1—leading front; diamonds, V_2—secondary front)

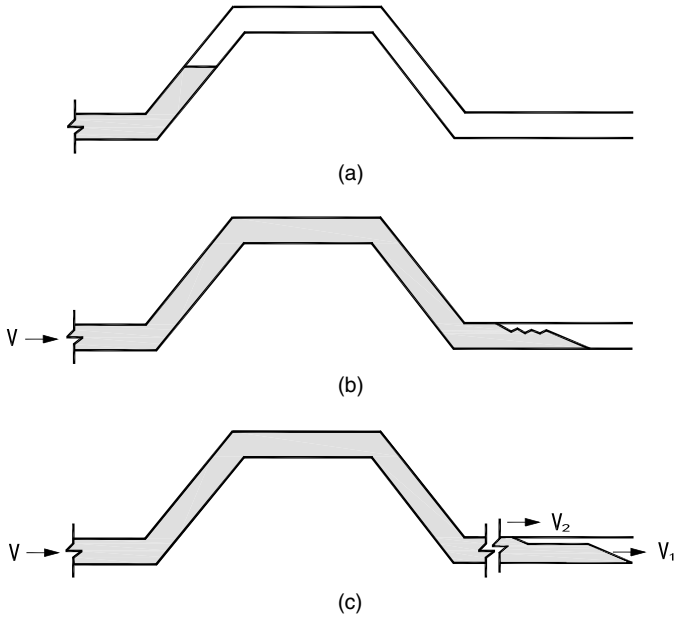

Fig. 6. Water front evolution in the filling process—the original water front splits into two fronts: (a) initial state; (b) early stage of filling; (c) propagation of two water fronts

Together with the inflow velocity, the measured water front velocities are shown in Fig. 5: the squares indicate V_1 and the diamonds V_2. The velocities V_1 and V_2 are the average velocities over the trajectory between two subsequent sections, and the symbols are plotted at the arrival times of the water fronts at the timing sections. Only the velocities that are determined from the water-level meters are presented in Fig. 5. The pressure transducers gave results close to those from the water-level measurements for the leading front (V_1), although they could not accurately sense the arrival of the secondary front (V_2) because of the small pressure rise associated with it. The water front starts at $x = -6.5$ m and has already split into two fronts when it arrives at section 1 ($x = 1.7$ m) so that velocities V_1 and V_2 are clearly different and the difference is more than 1 m/s, as shown in Fig. 5. Both water front velocities follow the trend of the inflow rate. The front arrival times at timing sections and corresponding velocities are listed in Tables 1 and 2. When the leading front is traveling between Section 3 ($x = 46.4$ m) and Section 9 ($x = 252.9$ m), the velocity difference between water column front (V_1) and tail (V) is approximately 0.4 m/s, except at Section 8 ($x = 206.8$ m), where it decreases to 0.24 m/s. Similarly, before the secondary front arrives at Section 9, the velocity difference between front (V_2) and tail (V) is approximately -1 m/s except at Section 8 ($x = 206.8$ m), where the difference increases to -1.25 m/s as a result of air pocket formation. The velocity variation at Section 8 is the result of a hydraulic jump that occurred between Sections 8 and 9, which is evident from the water-level measurements shown subsequently. The area between the velocity curves V_1 and V_2 (interpolated from Tables 1 and 2) is the amount of air intruded on top of the stratified flow. This is further examined at the end of the next section. Two water fronts were also observed by Vasconcelos et al. (2005) and presented by Guizani et al. (2006), however, without a quantitative analysis as made in this study.

Table 1. Location x, Arrival Time t, Average Velocity V_1, and Inflow Velocity V (at t_1) of the Leading Water Front

Section	x (m)	t_1 (s)	V_1	V (m/s)	$V_1 - V$
1	1.7	1.61 ± 0.07	5.09	2.61	2.48
3	46.4	9.12 ± 0.16	5.96	5.66	0.30
5	111.7	21.09 ± 0.36	5.46	5.05	0.41
7	183.7	35.28 ± 0.33	5.07	4.50	0.43
8	206.8	40.20 ± 0.35	4.70	4.36	0.24
9	252.9	50.34 ± 0.44	4.55	4.10	0.45

Table 2. Location x, Arrival Time t, Average Velocity V_2, and Inflow Velocity V (at t_2) of the Secondary Water Front

Section	x (m)	t_2 (s)	V_2	V (m/s)	$V - V_2$
1	1.7	5.44 ± 0.18	1.38	5.84	4.46
3	46.4	14.51 ± 0.25	4.92	5.30	0.38
5	111.7	32.48 ± 0.40	3.63	4.56	0.96
7	183.7	56.17 ± 0.59	3.04	4.00	0.96
8	206.8	64.39 ± 0.36	2.81	4.06	1.25
9	252.9	80.42 ± 0.41	2.87	4.03	1.16

Water Levels

The water-level measurements for three repeated runs in Fig. 7 show a good repeatability. The splitting of the water front is evident. The water levels at six locations in one typical run are shown in Fig. 8. Figs. 7 and 8 clearly show that the pipeline is not entirely empty at the beginning. Water is primarily present between Section 3 ($x = 46.6$ m) and Section 8 ($x = 206.8$ m), and its highest level is 35 mm at Section 5 ($x = 111.7$ m). The fact that there is water accumulation in the system before the filling is possibly the result of the sagging of the pipeline. That is, the elevation of the pipeline between Sections 3 ($x = 46.6$ m) and Section 8 ($x = 206.8$ m) is not zero as desired, but a small negative value. This condition differs from rapid filling tests with sloped pipelines as used by Liou and Hunt (1996) and Vasconcelos et al. (2005). As indicated by Arai and Yamamoto (2003), the pipeline slope could locally deviate from the targeted slope.

Fig. 8 indicates that the shape of the leading water front does not change much before it arrives at Section 9 ($x = 252.9$ m). Its final wedge length is approximately 3 m as estimated from the observed rise time (0.5–0.75 s) and the measured velocity. The wedge-shaped front [Figs. 8 and 6(c)] is initiated at the pipe bridge. As Fig. 7 shows, the water surface of the stratified flow is fluctuating [small burrs in Figs. 7(e and f) and large spikes in Figs. 7(a and d)], caused by local obstructions such as bridge and bends. This is consistent with the observation of Hamam and McCorquidale (1981) that even if there was no hydraulic jump in the sewer, the water surface was very unstable at relative depths $h/D > 0.8$, showing that the stratified flow was affected by geometric discontinuities.

However, for the long-term behavior, the average height of the leading water front is more or less constant (192 ± 8 mm) until it arrives at Section 9 ($x = 252.9$ m), where it increases to 230 mm. The secondary front reaches Section 1 ($x = 1.7$ m) at approximately $t = 5.4$ s. Its shape changes slightly with time. The average height of the secondary front is 43 ± 8 mm until it arrives at Section 8 ($x = 206.8$ m). It decreases to 6 mm at Section 9 ($x = 252.9$ m). The abrupt change in the height of the two water fronts at Section 9 indicates that a large flow-regime transition (hydraulic jump) must have occurred between Sections 8 ($x = 206.8$ m) and 9 ($x = 252.9$ m). The occurrence of a hydraulic jump is attributed to the reflection at the 90° elbow in combination with the stagnant layer of water ahead of the leading water front. The distance between the two water fronts $\Delta L = (V_1 - V_2)\Delta t$ increases with time. It is approximately 20 m when the secondary

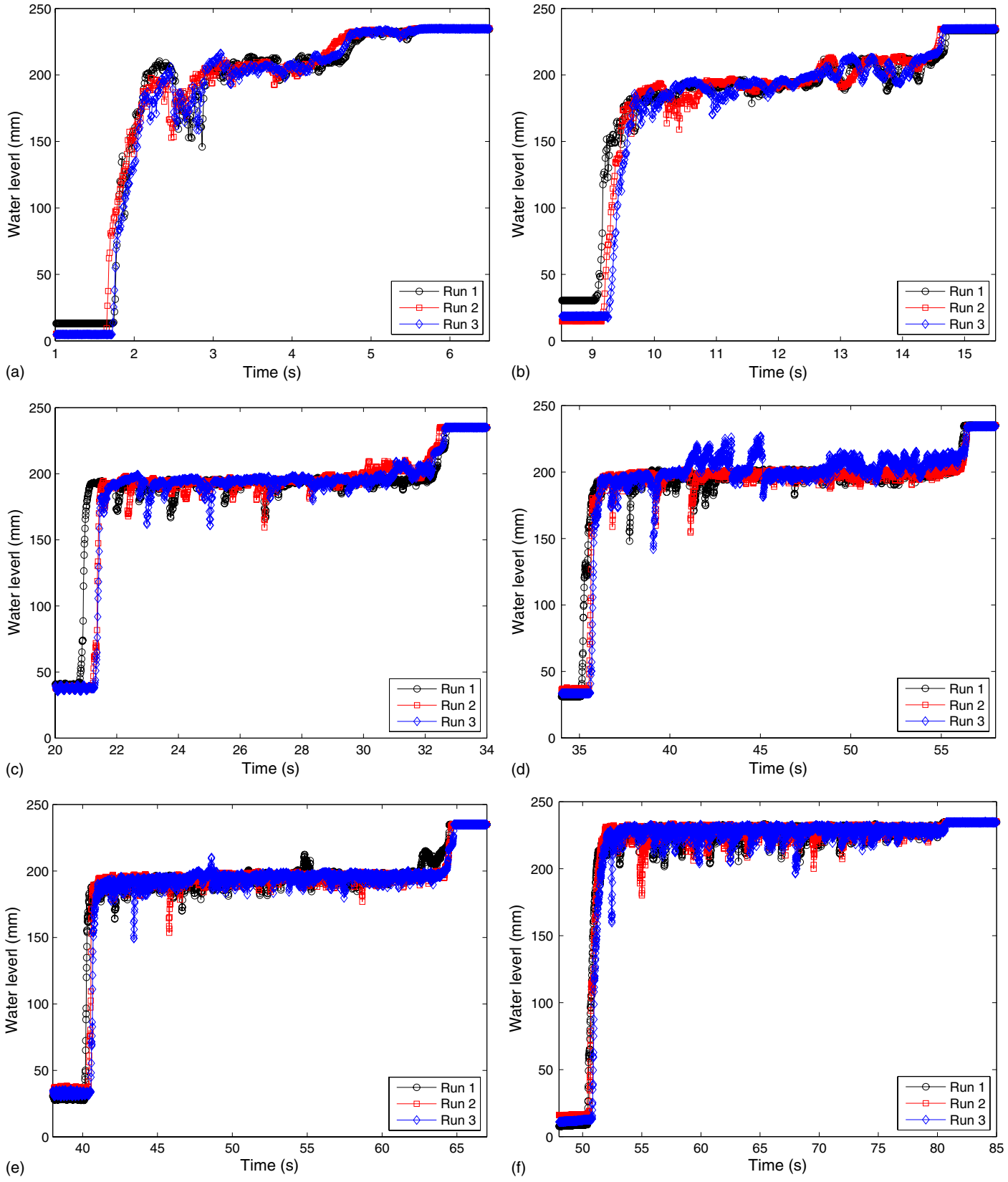

Fig. 7. Water levels at six different locations in three repeated filling runs: (a) WL1; (b) WL3; (c) WL5; (d) WL7; (e) WL8; (f) WL9 (see Table 1 and Fig. 2 for locations)

water front arrives at $x = 1.7$ m ($t = 5.4$ s), and it increases to 75 m when the leading water front arrives at $x = 206.8$ m at $t = 40.2$ s. According to these observations, a quantitative analysis of the water–air interface evolution is shown in Fig. 9.

Because of insufficient draining between two subsequent filling tests, most of the pipeline has an initial water depth (mainly from $x = 46.4$ m to $x = 206.8$ m and depth varying with the x coordinate). Generally, a sudden inflow in such a system will generate a

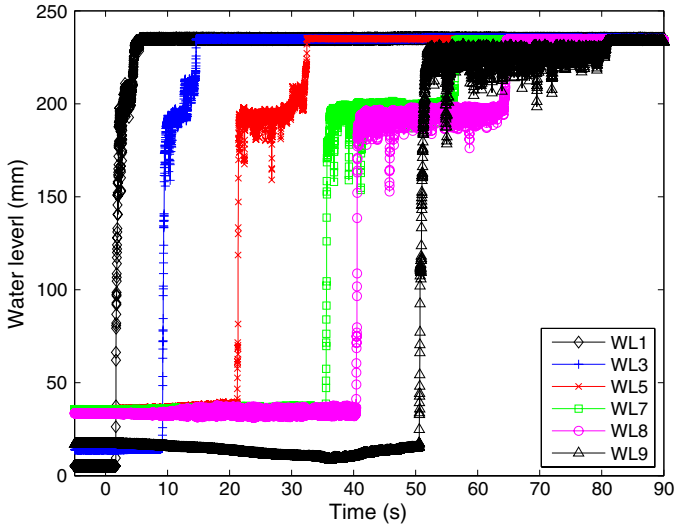

Fig. 8. Water-level changes at six different locations in one typical filling run

bore (planar) front (Henderson 1966) and not a feather-tip (wedge) front like the one indicated in Fig. 6. However, the images captured by the camera (Fig. 10) did not indicate a clear bore front. This is attributed to the pipe bridge, which produces a wedge-shaped front straight away, and to the relatively small water depth [less than 5% of the pipe diameter as shown in Fig. 7(f)] at the measuring site ($x = 249.5$ m, close to Section 9). The images captured at the transparent location ($x = 3.8$ m) are similar to those shown in Fig. 10 but with a higher flow velocity and hence smaller time scale. A recording at the transparent location ($x = 68.5$ m in Fig. 1) would have provided useful insights in this respect, but unfortunately this has not been done because of a lack of time. However, when zooming in on Fig. 7, the measured water-level rise caused by the leading water front at positions with relatively large initial water depth (e.g., $x = 111.7$ m and $x = 183.7$ m) is still a sort of linear wedge. The sampling rate of 100 Hz used in the experiments was sufficiently high to capture a planar bore front if it were there.

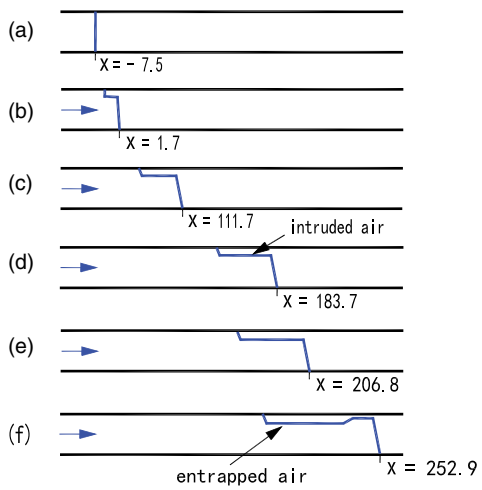

Fig. 9. Air intrusion in the filling experiments (m); the layer of intruded air lengthens, but its thickness does not change in stages (b), (c), (d), and (e). A hydraulic jump occurred between stages (e) and (f), after which entrapped air is gradually expelled from the system

Fig. 10. Water front evolution at $x = 249.5$ m in the filling process (snapshots by video camera with a 0.04-s time interval starting at $t = 50$ s)

The evolution of the leading water front involves the intrusion of air. When the leading water front has reached Section 9 ($x = 252.9$ m) at $t = 50.3$ s, the pipe at Section 7 ($x = 183.7$ m) is still not full (Fig. 8). The thickness of the air layer between the two water fronts is more or less constant before the occurrence of the hydraulic jump. The length of the air layer increases with time at rate $V_1 - V_2$, the average value of which is 1.45 m/s in the time interval between $t = 5.4$ s and $t = 40.2$ s (Tables 1 and 2). A theoretical prediction of $V_1 - V_2$ is given in Appendix I. Consequently, the increased length of the air layer within that time interval is $1.45 \times (40.2 - 5.4) = 50.5$ m, which is consistent with the estimate made previously (75 m − 20 m = 55 m).

Based on the heights of the water fronts shown in Figs. 7 and 8 and together with Fig. 5 and Tables 1 and 2, the conservation of volume at the moment the leading water front arrives at Section 5 ($x = 111.7$ m, $t = 21$ s) is checked. The measured inflow rate is $Q_{\text{in}} = VA = 5.05 \times 0.0435 = 0.22$ m^3/s. The volume change at the water fronts is $Q_{\text{out}} = V_1A_1 + V_2A_2 = 5.46 \times 0.0381 + 4.5 \times 0.0054 = 0.23$ m^3/s. Areas A_1 and A_2 correspond to a measured water level of 192 mm. Velocity V_1 is taken from Table 1 and velocity V_2 is interpolated from Table 2. Approximately Q_{in} equals Q_{out}. Thus, the conservation of volume and corresponding measurements are verified.

The volume of the layer of intruded air is also checked. When the leading front arrives at WL8 ($x = 206.8$ m, $t = 40.2$ s), the volume of the water (area under the inflow rate curve between $t = 0$ and $t = 40.2$ s plus the volume of initially present water) is $\forall_1 = 8{,}790$ L. The initial voided pipe volume is $\forall_2 = LA = (206.8 + 6.5) \times 0.0435 \times 10^3 = 9{,}280L$. Hence, the volume of

the intruded air $\forall_{air} = \forall_2 - \forall_1 = 490$ L. Alternatively, using the measured water level (192 mm) to calculate $\forall_{air}$, the air on top of the horizontal water surface is found to be $\forall_{air} = A_2 \Delta L = 0.0054 \times 10^3 \times 75 = 410$ L. The air volume on top of the wedge-shaped water front is approximately 60 L as estimated from the 3-m-long front. Consequently, the intruded air volumes calculated from the two approaches are approximately the same. The small discrepancy is because of the measuring error and the waviness of the free surface [spikes in WL8, Fig. 7(e)]. This verification confirms the water-level measurements.

Pressures

Pressure histories at different locations along the PVC pipeline are shown in Fig. 11. When the leading water front arrives at the downstream bend ($x = 267$ m) at $t = 54$ s, the recorded pressures show severe oscillations because of the slug effect at the elbow and consequently at the outlet. The amplitude of the oscillation at Section 9 ($x = 252.9$ m) is approximately 0.1 barg, which is approximately equal to $0.5\rho V_1^2 \approx 0.5 \times 1000 \times 4.5^2/10^5 \approx 0.1$ barg. As shown in Fig. 11, the magnitude and damping time of the pressure oscillation is amplified in the readings at transducers p_5 ($x = 111.7$ m) and p_{3b} ($x = 46.6$ m, pipe bottom). This response is physically impossible unless, for example, the compression of an entrapped air pocket gives rise to it. One possibility is that some air was entrapped between the 180° turn and the transducer p_5. This is consistent with the measurement of the WL meter 7, as the secondary front has not yet arrived at Section 7 ($x = 183.7$ m) at time $t = 54$ s [Fig. 7(d)].

The pressure histories of transducers p_u ($x = -14$ m) and p_{uv} ($x = -27.7$ m) are shown in Fig. 12 together with p_1 ($x = 1.6$ m), p_{3b} ($x = 46.6$ m, pipe bottom), and p_{3t} ($x = 46.6$ m, pipe top). The small pressure difference between p_{3b} and p_{3t} is the result of the elevation difference D_{PVC}. The nearly same pressure at the bottom and top confirms a uniform pressure distribution in a cross section. The difference between the pressure rise times of p_{3b} and p_{3t} is approximately 0.8 s, which is much smaller than the time difference between the arrival of the two water fronts [approximately 5.4 s as shown in Fig. 7(b)]. This suggests the pressurization of the intruded air as detailed subsequently. At the beginning of the filling process, p_u and p_{uv} experience a rapid rise

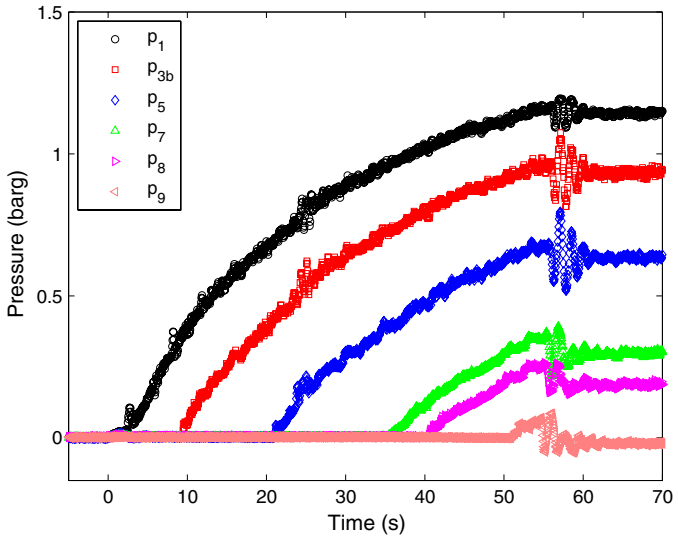

Fig. 11. Pressure history at six different locations along the PVC test section in one typical run (see Fig. 1 for locations)

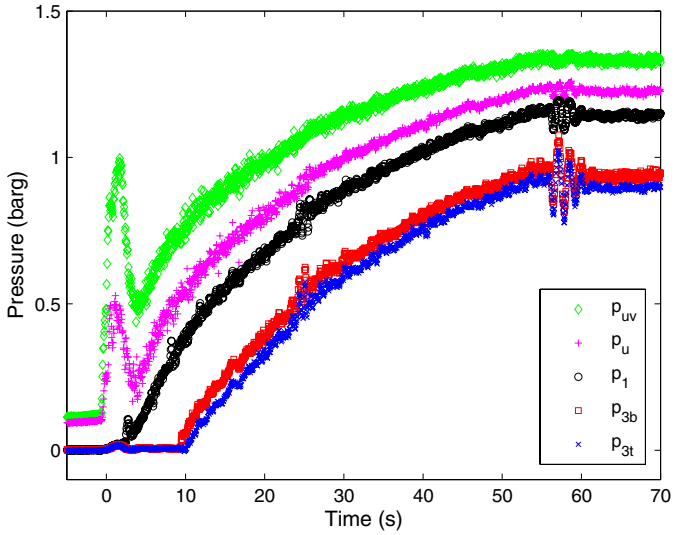

Fig. 12. Pressure history at $x = -27.7$ m (p_{uv}), -14 m (p_u), 1.6 m (p_1), and 46.6 m (p_3) in a typical filling run

and fall (short-lived peak for 3 s) and then gradually increase as p_1 and p_3 do. The peak in p_u and p_{uv} may be attributed to compressing and decompressing of the air entrapped between the Y-junction ($x = -27.2$ m) and the check valve ($x = -43.1$ m). This peak in driving pressure can be (part of) the reason for the short-lived flow-rate peak between $t = 4$ s and $t = 6$ s (Fig. 5).

When comparing Fig. 11 with the water-level measurements in Figs. 7 and 8, the air layer on top of the water column (Fig. 9) is clearly not under atmospheric pressure. This is evident from the following three aspects. First, the air pressure rise has been clearly detected by the pressure sensor p_{3t}. Before the secondary front arrived at Section 3 ($x = 46.6$ m) at $t = 14.5$ s [Fig. 7(b)], the head increase at the pipe crown was approximately 2 m (0.2 barg as shown in Fig. 12), which is 10 times the water level (hydrostatic head at bottom) and certainly not atmospheric. Second, it is demonstrated by the combined water-level and pressure measurements. Fig. 7(d) shows that there was air on top of the stratified flow at WL7 between 35 and 55 s. The pressure rise recorded by the downstream sensors 8 ($x = 206.8$ m) and 9 ($x = 252.9$ m) started from 40.5 s [Fig. 11 and more clearly Fig. 13(b)] and 51 s (Fig. 11), respectively. When station WL7 ($x = 183.7$ m) became full at time 55 s, the pressure head at Section 8 ($x = 206.8$ m) was already 2.5 m (10 times D). Third, Fig. 7(e) shows that the water level at Section 8 ($x = 206.8$ m) was approximately 192 mm in the time interval between 40 and 65 s. For the air on top to be at atmospheric pressure, the hydrostatic pressure head measured at Section 8 should be approximately 192 mm $-D_{PVC}/2 \approx 74$ mm during that time interval. This clearly differs from the measurement of p_8 ($x = 206.8$ m) as shown in Fig. 13(b), and demonstrates that the intruded air is under pressure higher than atmospheric. The rapid acceleration is associated with axial pressure gradients that are much larger than any vertical (hydrostatic) pressure gradients. In spite of this, the air ahead of the leading water front is still under atmospheric conditions because of the open outlet and its low density. For example, before the leading water front arrived at Section 7 ($x = 183.7$ m) at $t = 32$ s, the pressure at Section 7 and ahead was zero (Fig. 11).

The pressure distributions (hydraulic grade lines) at three instants are shown in Fig. 14. The chosen times are the instants when the leading water front arrives at the transducers p_5 ($x = 111.7$ m), p_7 ($x = 183.7$ m), and p_9 ($x = 252.8$ m). The linear pressure distribution along the water column indicates a uniform pressure

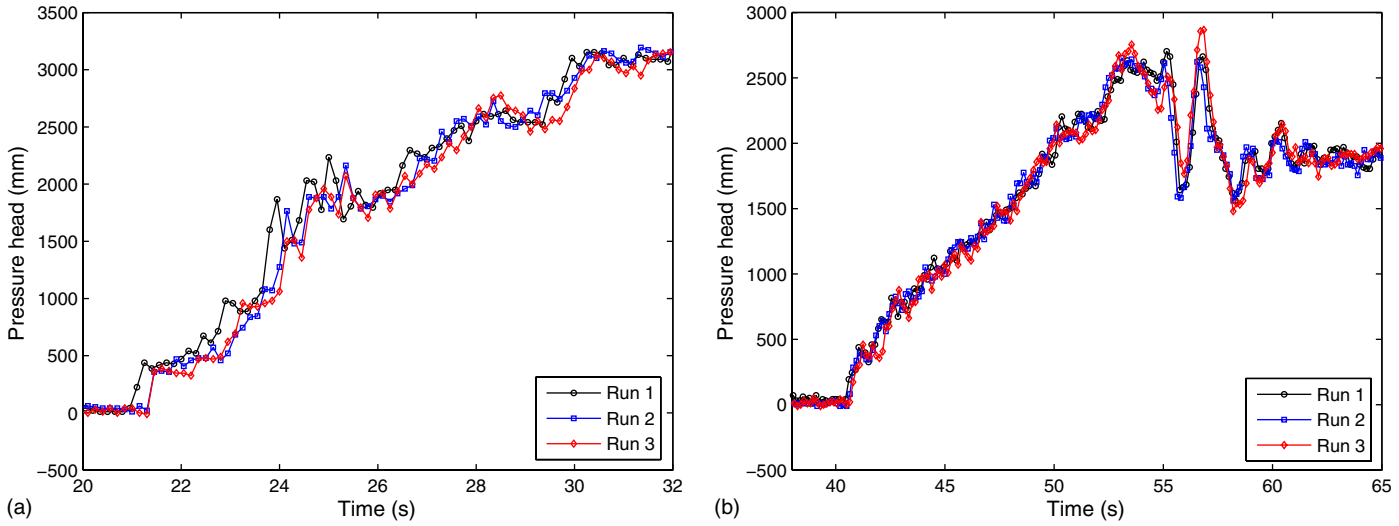

Fig. 13. Pressure history at two locations along the PVC test section in three repeated filling runs: (a) Section 5 ($x = 111.7$ m); (b) Section 8 ($x = 206.8$ m)

gradient that decreases in time. It implies that the advancing water column behaves like a rigid column, despite the air intrusion that takes place. It also confirms the previous observation of nonatmospheric air intrusion, because if the intruded air were under atmospheric pressure, the pressure distribution would not be linear up to the leading front (but up to the secondary front). This can be further clarified as follows. When the leading water front arrives at Section 9 ($x = 252.8$ m), the secondary water front has not yet arrived at Section 7 ($x = 183.7$ m) (Fig. 8). If the intruded air would be under atmospheric pressure, the pressure gradient between Sections 7 and 9 would be close to zero. This is apparently not the case as shown in Fig. 14. The pressure head increases with time until the steady state is achieved. This agrees with the results shown in Fig. 11.

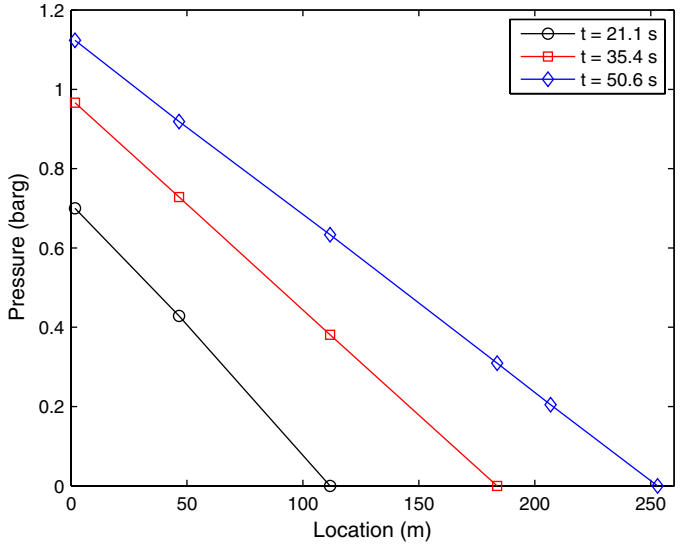

Fig. 14. Pressure distribution along the water column at three time instants: when the leading water front arrives at Section 5 ($x = 111.7$ m) (circles), Section 7 ($x = 183.7$ m) (squares), and Section 9 ($x = 252.9$ m) (diamonds); the x-coordinates of the symbols are the locations of the pressure transducers

Numerical Simulation

To model rapid filling of pipelines with initially entrapped air, end orifice or ventilation conditions, many researchers have applied the rigid-column theory (Cabrera et al. 1992; Liou and Hunt 1996; Cabrera et al. 1997; Izquierdo et al. 1999; Trajkovic et al. 1999; Lee and Martin 1999; Zhou 2000; Liu and Suo 2004; Martin and Lee 2012) and developed other sophisticated mathematical models and corresponding numerical techniques (Vasconcelos et al. 2005; Lee 2005; Zhou et al. 2011; Hou et al. 2012b; Zhou et al. 2013a, b; Trindade and Vasconcelos 2013). Although the primary objective of this paper is to present the experimental results, the potential significance of these can be illustrated by comparison with the existing state of the art in the modeling of rapid pipe filling. This study focuses on the rapid filling of an initially empty pipeline with an open end as experimentally examined previously, for which rigid-column theory governed by a set of ordinary differential equation (ODEs) is commonly used. The rigid-column model for filling pipes in series was formulated by Liou and Hunt (1996). The model describes the motion of a lengthening water column advancing in an undulating pipeline. As shown by Axworthy and Karney (1997), the filling process can be calculated more efficiently by eliminating the pressure head at the pipe-segment junctions from the momentum equation. This technique was recently extended to represent branched systems (Razak and Karney 2008). The rigid-column model gives good results as long as the flow remains axially uniform. When the water column is abruptly disturbed somewhere in the system, pressure oscillations along its length, or even column separation, may result and then the rigid-column model fails. The elastic model governed by a set of partial differential equations (PDEs) (water-hammer equations with moving boundaries) is needed to simulate extremely rapid filling processes (Malekpour and Karney 2008). The numerical difficulty is in the moving boundary. An attempt to tackle it within the fully implicit box (or Preismann) finite-difference scheme was made by Malekpour and Karney (2008). Because a fixed spatial grid and an adaptive temporal grid are used in this scheme, the Courant number is time-dependent. An uncontrollable large Courant number caused serious convergence problems. To overcome it, the method of characteristics (MOC) was applied (Malekpour and Karney 2011). Because both the spatial and temporal grid are fixed

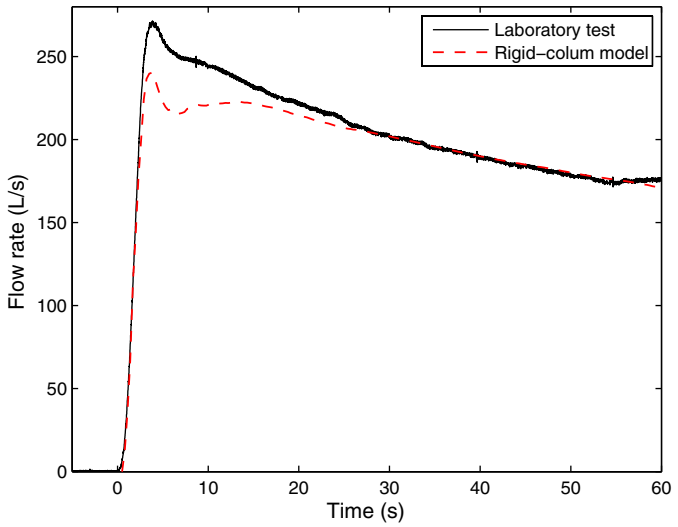

Fig. 15. Flow rate history in experiment (solid line) and numerical simulation (dashed line)

in the conventional MOC, the Courant number is constant and an interpolation had to be used to deal with the increasing length of the water column. Recently, the Lagrangian particle smoothed particle hydrodynamics (SPH) method was applied to solve the elastic model (Hou et al. 2012b), which is particularly suitable for problems with moving boundaries. For the case of large-scale pipeline emptying with compressed air supplied from the upstream end, the influence of the driving air pressure and downstream valve resistance on the outflow rates was studied by Laanearu et al. (2012). Noninertial reference-frame control-volume models were used to explain the phenomena observed. However, the coefficients in the model were calibrated from the specific experimental results by means of curve fitting, by neglecting the water-hammer oscillations.

The rigid-column model developed by Liou and Hunt (1996) with the efficient computation of Axworthy and Karney (1997) is applied in this study to simulate the experimental results (Appendix II). The location of the pressure transducer p_u ($x = -14$ m) is taken as the upstream boundary of the water column and the measured pressure there (Fig. 12) is applied as the driving pressure. The elevation profile (pipe bridge and siphon) is included in the calculation. The initial water column length is $L_0 = 14 - 6.5 = 7.5$ m. The friction factor is $f = 0.0136$. The pipe is assumed to be initially empty, and air intrusion is disregarded. The simulation is terminated after the water front arrives at the end of the pipeline ($x = 272.1$ m).

The one-dimensional rigid-column solution is compared with the laboratory test in Fig. 15. The predicted flow rate history has the same trend as the experiment. The recorded short-lived peak at $t = 4$ s is the result of the initial peak in the driving pressure p_u ($x = -14$ m), as shown in Fig. 12. The deviation of the flow maximum is attributed to the three-dimensional effect of the pipe bridge (free overflow) and the air intrusion. It was found that the peak of the numerical flow rate is rather sensitive to the length of the upstream leg of the bridge. In addition, as mentioned previously, the response time of the pressure transducer is approximately 1 s quicker than the flow meter. This gives some flexibility in choosing the starting time of the driving pressure p_u ($x = -14$ m) in Fig. 12.

The global agreement between the rigid-column solution and the pipeline fast-filling experimental result implies that air intrusion is of less importance for the overall filling process. An important reason is that the friction mechanism in stratified flow is more or less equivalent to that in the assumed rigid-column filling of the entire pipe cross-section. The observed fact that the intruded air is under pressure resulting in a linear pressure distribution along the entire (stratified and full) water column may play a role too.

Conclusions

A 300-m-long primarily horizontal pipeline of 250-mm diameter was filled with water within 1 min. The filling process was repeated more than 70 times and fully recorded by flow meters, pressure transducers, water-level meters, and void fraction meters. The experiments resulted in a detailed data set for the investigation of unsteady pipe flows with water–air interface propagation. From the examination of the measurements it is concluded that:

1. The filling process was characterized by two stages. After the sudden opening of the upstream valve and under the driving reservoir pressure, the flow quickly accelerated and reached its maximum discharge. The filling process then followed a period of slowly decreasing discharge as a result of increasing pipe friction and increasing water mass until a steady state was reached.
2. The initial static water front (water–air interface) split into two fronts because of the pipe bridge (free overfall), the velocities of which followed the inflow velocity. The stratified flow between the two water fronts had a nearly constant thickness before the occurrence of a hydraulic jump.
3. Water hammer as a result of the rapid opening of the upstream valve did not affect the overall filling process because the initial water column was short compared with the pipeline length. The pressure at each location increased smoothly as a concave-down curve until a steady state was reached. The pressure distribution along the water column was linear, and its slope decreased with time because of its increasing length and its deceleration. This implies that the water flow during filling behaved as a rigid column, although a flow regime transition occurred.
4. Flow stratification and nonplanar water fronts have been observed. These are of key importance for the dynamic forces on bends. The authors are fully aware of this because they had serious problems with fixing the most downstream bend.
5. The pressure of the air on top of the water column was under a pressure higher than atmospheric. This implies that a single local pressure transducer is not sufficient to measure the water level in stratified internal flow.
6. A basic one-dimensional rigid-column simulation showed acceptable agreement with the measured inflow rate. Consequently, it also gave a reasonable estimate of the velocity of the leading water front. The velocity of the secondary water front agreed with a prediction by standard wave theory.

Appendix I. Speed of Propagation of Disturbances in Circular Channel Flow

The filling process is characterized by a leading water front propagating at speed V_1 and a secondary front propagating at speed V_2, as sketched in Fig. 6(c). Alternatively, the secondary front can be regarded as a disturbance propagating on top of the leading water column. The disturbance travels at speed $V_1 - V_2$ in upstream direction. The theoretical speed of propagation is (Wiggert 1972)

$$c = \sqrt{g\frac{A}{W_t}} \tag{1}$$

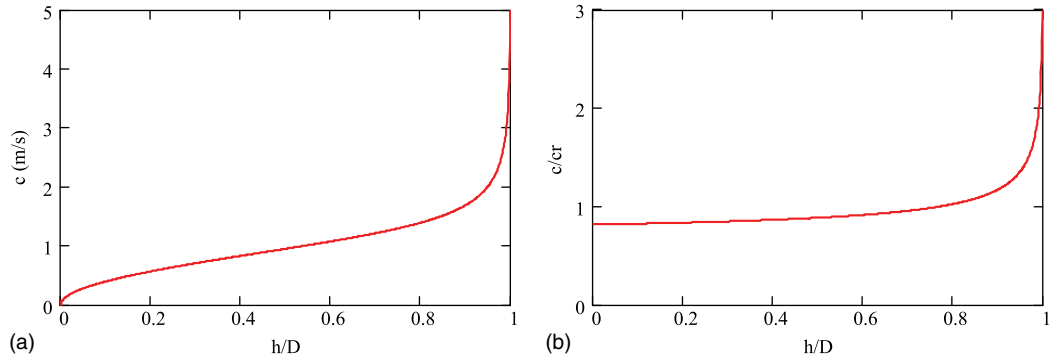

Fig. 16. Speed of propagation c as a function of water depth h: (a) dimensional for $D = 0.235$ m; (b) dimensionless (independent of D)

where A and W_t = area and top width of the prismatic flow section, respectively, and $g = 9.81$ m/s^2 is the gravitational acceleration. For a circular channel

$$A(\xi) = \frac{1}{8}\pi D^2\left[1 + \frac{2}{\pi}\arcsin(2\xi - 1) + \frac{4}{\pi}(2\xi - 1)\sqrt{\xi - \xi^2}\right] \quad (2)$$

and

$$W_t(\xi) = 2D\sqrt{\xi - \xi^2} \quad (3)$$

where $\xi = h/D$ = ratio of water depth and pipe diameter. The dependence of propagation speed c on dimensionless water-depth ξ for a pipe with an inner diameter of 0.235 m is shown in Fig. 16(a). For a water depth $h = 0.192$ m, the speed is $c = 1.43$ m/s, which compares very well with $V_1 - V_2 = 1.45$ m/s, estimated from Tables 1 and 2. It is approximately the speed of propagation in a rectangular channel: $c_r = \sqrt{g/h} = 1.37$ m/s. The dimensionless speed c/c_r is displayed in Fig. 16(b), which gives the deviation of speed in a circular channel from that in a rectangular channel. For $h/D < 0.769$ the speed in a circular channel is lower; otherwise it is higher.

Eq. (1) has been derived for stationary flow with hydrostatic pressures. Both conditions are violated in the experiments described in this study.

Appendix II. Rigid-Column Model

Based on the developments by Liou and Hunt (1996) and Axworthy and Karney (1997), a one-dimensional mathematical model has been established and implemented. Four assumptions state that the pipe cross section remains full during filling, that the pressure at the front is atmospheric, that the water-pipe system is incompressible (i.e., rigid water column), and that the friction is quasi-steady. Define H_i as the head at the downstream end of pipe i. Suppose that the water front is traveling in the $(i + 1)$th pipe as shown in Fig. 17. Applying Newton's law of motion to the advancing water column in the $(i + 1)$th pipe yields

$$\frac{l(t)}{gA_{i+1}}\frac{dQ}{dt} = H_i - \frac{f_{i+1}l(t)}{D_{i+1}}\frac{Q^2}{2gA_{i+1}^2} + l(t)\sin\theta_{i+1} \quad (4)$$

where $l(t)$ = length of the water column in the partially filled pipe; θ = angle downward from the horizontal; f = Darcy-Weisbach friction factor; $A = \pi D^2/4$ is the pipe cross-sectional area; and $Q = VA$ is the uniform flow rate. Similarly, the fully filled upstream pipes yield the following:

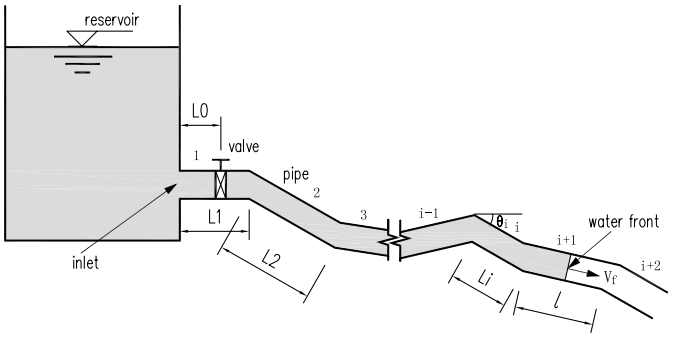

Fig. 17. Filling of a pipeline with undulating elevation profile

$$\frac{L_j}{gA_j}\frac{dQ}{dt} = H_{j-1} - H_j - \frac{f_jL_j}{D_j}\frac{Q^2}{2gA_j^2} + L_j\sin\theta_j, \quad j = 2, \ldots, i \quad (5)$$

where i depends on t. Because of entrance head loss and velocity head at the inlet, the equation for the first pipe is slightly different, as follows:

$$\frac{L_1}{gA_1}\frac{dQ}{dt} = H_R - H_1 - \left(K + 1 + \frac{f_1L_1}{D_1}\right)\frac{Q^2}{2gA_1^2} + L_1\sin\theta_1 \quad (6)$$

where H_R = reservoir head; and K = entrance loss coefficient. By adding Eqs. (4)–(6), all interior heads H_j $(j = 1, \ldots, i)$ are canceled, and one equation is obtained for the filling discharge Q

$$\frac{1}{g}\left[\sum_{j=1}^{i}\frac{L_j}{A_j} + \frac{l(t)}{A_{i+1}}\right]\frac{dQ}{dt} = H_R - \left[\sum_{j=1}^{i}\frac{f_jL_j}{D_jA_j^2} + \frac{f_{i+1}l(t)}{D_{i+1}A_{i+1}^2} + \frac{K+1}{A_1^2}\right]\frac{Q^2}{2g} + \sum_{j=1}^{i}L_j\sin\theta_j + l(t)\sin\theta_{i+1} \quad (7)$$

Substituting the total length of the water column $L(t)$

$$L(t) = \sum_{j=1}^{i}L_j + l(t) \quad (8)$$

into Eq. (7) gives

$$\frac{1}{g}[C_1L(t)+C_2]\frac{dQ}{dt}=H_R-[C_3L(t)+C_4+C_7]\frac{Q^2}{2g}+C_5L(t)+C_6 \tag{9}$$

where the time-dependent (because of i) coefficients $C_k(k=1,\ldots,7)$ are defined as

$$C_1=\frac{1}{A_{i+1}},\qquad C_2=\sum_{j=1}^{i}\frac{L_j}{A_j}-C_1\sum_{j=1}^{i}L_j,$$

$$C_3=\frac{f_{i+1}}{D_{i+1}A_{i+1}^2},\qquad C_4=\sum_{j=1}^{i}\frac{f_jL_j}{D_jA_j^2}-C_3\sum_{j=1}^{i}L_j,$$

$$C_5=\sin\theta_{i+1},\quad C_6=\sum_{j=1}^{i}L_j\sin\theta_j-C_5\sum_{j=1}^{i}L_j,\quad C_7=\frac{K+1}{A_1^2}$$

The total water column length is related to flow rate Q by

$$L=L_0+\int_0^t\frac{Q}{A_{i+1}}dt \tag{10}$$

where $L_0(<L_1)$ = initial column length at $t=0$ in Pipe 1. In Eqs. (9) and (10), i is the index of the latest pipe that has been fully filled. It starts from 0, indicating that Pipe 1 is partially filled. When $L(t)$ becomes larger than L_1, i becomes 1. When $L(t)$ becomes larger than L_1+L_2, i becomes 2, and so on.

Next, Eqs. (9) and (10) are solved for the two unknowns, Q and L. Eq. (9) is an ODE with the initial condition

$$Q(0)=0 \tag{11}$$

Eq. (10) is an integral equation in which A_{i+1} depends on time. ODE Eq. (9) is integrated with the fourth-order Runge-Kutta method and Eq. (10) with Simpson's rule.

Acknowledgments

The project *Transient vaporous and gaseous cavitation in pipelines* carried out at Deltares, Delft, the Netherlands, was funded through EC-HYDRALAB III Contract 022441 (R113) by the European Union. The authors like to express their sincere gratitude to staff at Deltares: Dr. Arno Kruisbrink, Dr. Christof Lubbers, and Dr. Hugo Hartmann for their help in the preparation of the project HYIII-Delft-4; and Richard Tuin, Martin Boele, and Theo Ammerlaan for their expert technical advices during the measurement periods. The first author is grateful to the China Scholarship Council (CSC) for financially supporting his Ph.D. studies at Eindhoven University of Technology, the Netherlands. The support in part by the National Natural Science Foundation of China (No. 61233009) and National Basic Research Program of China (No. 2013CB329301) is highly appreciated too. The sixth author gratefully acknowledges the support of the Slovenian Research Agency.

Notation

The following symbols are used in this paper:

A = cross-sectional area (m^2);
C_i = ith coefficient in Eq. (9);
c = wave propagation speed (m/s);
D = pipe inner diameter (m);
f = Darcy-Weisbach friction factor (-);
g = gravitational acceleration (m/s^2);
H = head (m);
H_R = reservoir head (m);
h = water depth (m);
h_f = friction head loss (m);
h_{lb} = local head loss resulting from long bend (m);
i,j = index;
K = head-loss coefficient (-);
l,L = length (m);
p = pressure (barg);
R = elbow radius of curvature (m);
T = temperature (°C);
V = velocity (m/s);
Vi = ith valve;
W = width (m);
x,y,z = coordinate (m);
θ = angle (°);
ξ = dimensionless depth (-);
ρ = mass density (kg/m^3); and
$\forall$ = volume (m^3).

References

Arai, K., and Yamamoto, K. (2003). "Transient analysis of mixed free-surface-pressurized flows with modified slot model (Part1: Computational model and experiment)." *Proc., 4th ASME-JSME Joint Fluids Summer Engineering Conf.*, ASME, New York.

Axworthy, D. H., and Karney, B. W. (1997). "Discussion of 'Filling of pipelines with undulating elevation profiles,' by Liou, C. P. and Hunt, W. A." *J. Hydraul. Eng.*, 10.1061/(ASCE)0733-9429(1997)123:12(1170), 1170–1174.

Bergant, A., et al. (2010). "Water hammer and column separation due to accidental simultaneous closure of control valves in a large scale two-phase flow experimental test rig." *Proc., Pressure Vessels & Piping Division / K-PVP Conf.*, Vol. 3, ASME, New York, 923–932.

Bergant, A., Hou, Q., Keramat, A., and Tijsseling, A. S. (2011). "Experimental and numerical analysis of water hammer in a large-scale PVC pipeline apparatus." *Proc., 4th Int. Meeting on Cavitation and Dynamic Problems in Hydraulic Machinery and Systems*, IAHR, Univ. of Belgrade, Belgrade, Serbia, 27–36.

Cabrera, E., Abreu, J., Perez, R., and Vela, A. (1992). "Influence of liquid length variation in hydraulic transients." *J. Hydraul. Eng.*, 10.1061/(ASCE)0733-9429(1992)118:12(1639), 1639–1650.

Cabrera, E., Izquierdo, J., Abreu, J., and Iglesias, P. L. (1997). "Discussion of 'Filling of pipelines with undulating elevation profiles,' by Liou, C. P. and Hunt, W. A." *J. Hydraul. Eng.*, 10.1061/(ASCE)0733-9429(1997)123:12(1170.2), 1170–1174.

De Martino, G., Fontana, N., and Giugni, M. (2008). "Transient flow caused by air expulsion through an orifice." *J. Hydraul. Eng.*, 10.1061/(ASCE)0733-9429(2008)134:9(1395), 1395–1399.

Guizani, M., Vasconcelos, J. G., Wright, S. J., and Maalel, K. (2006). "Investigation of rapid filling in empty pipes." *Intelligent modeling of urban water systems, monograph 14*, W. James, K. N. Irvine, E. A. McBean, and R. E. Pitt, eds., CHI, Guelph, ON, Canada.

Guo, Q., and Song, C. S. S. (1990). "Surging in urban storm drainage systems." *J. Hydraul. Eng.*, 10.1061/(ASCE)0733-9429(1990)116:12(1523), 1523–1537.

Hamam, M. A., and McCorquidale, J. A. (1981). "Transition of gravity to surcharge flow in sewers." *Proc., Int. Symp. on Urban Hydrology, Hydraulics and Sediment Control*, Univ. of Kentucky, Lexington, KY, 173–177.

Henderson, F. M. (1966). *Open channel flow*, Macmillan, New York.

Hou, Q. (2012). "Simulating unsteady conduit flows with smoothed particle hydrodynamics." Ph.D. thesis, Eindhoven Univ. of Technology, Eindhoven, the Netherlands.

Hou, Q., et al. (2012a). "Experimental study of filling and emptying of a large-scale pipeline." *CASA Rep, 12-15*, Eindhoven Univ. of Technology, the Netherlands.

Hou, Q., Zhang, L. X., Tijsseling, A. S., and Kruisbrink, A. C. H. (2012b). "Rapid filling of pipelines with the SPH particle method." *Procedia Eng.*, 31, 38–43.

Izquierdo, J., Fuertes, V. S., Cabrera, E., Iglesias, P. L., and Carcía-Serra, J. (1999). "Pipeline start-up with entrapped air." *J. Hydraul. Res.*, 37(5), 579–590.

Keramat, A., Tijsseling, A. S., Hou, Q., and Ahmadi, A. (2012). "Fluid-structure interaction with pipe-wall viscoelasticity during water hammer." *J. Fluid. Struct.*, 28(1), 434–455.

Laanearu, J., et al. (2012). "Emptying of large-scale pipeline by pressurized air." *J. Hydraul. Eng.*, 10.1061/(ASCE)HY.1943-7900.0000631, 1090–1100.

Laanearu, J., Bergant, A., Annus, I., Koppel, T., and van 't Westende, J. M. C. (2009). "Some aspects of fluid elasticity related to filling and emptying of large-scale pipeline." *Proc., 3rd Int. Meeting on Cavitation and Dynamic Problems in Hydraulic Machinery and Systems*, International Association of Hydrologic Repears (IAHR), Brno Univ. of Technology, Brno, Czech Republic, 465–474.

Laanearu, J., and van 't Westende, J. M. C. (2010). "Hydraulic characteristics of test rig used in filling and emptying experiments of large-scale pipeline." *Proc., Hydralab III Joint Transnational Access User Meeting*, Forschungszentrum Küste FZK, Hannover, Germany, 5–8.

Lee, N. H. (2005). "Effect of pressurization and expulsion of entrapped air in pipelines." Ph.D. thesis, Georgia Institute of Technology, Atlanta, GA.

Lee, N. H., and Martin, C. S. (1999). "Experimental and analytical investigation of entrapped air in a horizontal pipe." *Proc., 3rd ASME-JSME Joint Fluids Summer Engineering Conf.*, ASME, New York.

Liou, C. P., and Hunt, W. A. (1996). "Filling of pipelines with undulating elevation profiles." *J. Hydraul. Eng.*, 10.1061/(ASCE)0733-9429(1996)122:10(534), 534–539.

Liu, D. Y., and Suo, L. S. (2004). "Rigid model for transient flow in pressurized pipe system containing trapped air mass." *Adv. Water Sci.*, 15(6), 717–721 (in Chinese).

Lubbers, C. L. (2007). "On gas pockets in wastewater pressure mains and their effect on hydraulic performance." Ph.D. thesis, Delft Univ. of Technology, Delft, the Netherlands.

Malekpour, A., and Karney, B. W. (2008). "Rapidly filling analysis of pipelines using an elastic model." *Proc., 10th Int. Conf. on Pressure Surges*, BHR Group, Cranfield, U.K., 539–552.

Malekpour, A., and Karney, B. W. (2011). "Rapid filling analysis of pipelines with undulating profiles by the method of characteristics." *ISRN Appl. Math.*, 16.

Martin, C. S. (1976). "Entrapped air in pipelines." *Proc., 2nd Int. Conf. on Pressure Surges*, BHR Group, Bedford, U.K., 15–27.

Martin, C. S., and Lee, N. (2012). "Measurement and rigid column analysis of expulsion of entrapped air from a horizontal pipe with an exit orifice." *Proc., 11th Int. Conf. on Pressure Surges*, BHR Group, Bedford, U.K., 527–542.

Nydal, O. J., and Andreussi, P. (1991). "Gas entrainment in a long liquid slug advancing in a near horizontal pipe." *Int. J. Multiphase Flow*, 17(2), 179–189.

Ocasio, J. A. (1976). "Pressure surging associated with pressurization of pipelines containing entrapped air." *Special M.S. Research Rep.*, School of Civil Engineering, Georgia Institute of Technology, Atlanta, GA.

Razak, T., and Karney, B. W. (2008). "Filling of branched pipelines with undulating elevation profiles." *Proc., 10th Int. Conf. on Pressure Surges*, BHR Group, Cranfield, U.K., 473–487.

Tijsseling, A. S. (1996). "Fluid-structure interaction in liquid-filled pipe systems: A review." *J. Fluid. Struct.*, 10(2), 109–146.

Trajkovic, B., Ivetic, M., Calomino, F., and D'Ippolito, A. (1999). "Investigation of transition from free surface to pressurized flow in a circular pipe." *Water Sci. Technol.*, 39(9), 105–112.

Trindade, B. C., and Vasconcelos, J. G. (2013). "Modeling of water pipeline filling events accounting for air phase interactions." *J. Hydraul. Eng.*, 10.1061/(ASCE)HY.1943-7900.0000757, 921–934.

Vasconcelos, J. G. (2005). "Dynamic approach to the description of flow regime transition in stormwater systems." Ph.D. thesis, Univ. of Michigan, Ann Arbor, MI.

Vasconcelos, J. G., and Wright, S. J. (2005). "Experimental investigation of surges in a stormwater storage tunnel." *J. Hydraul. Eng.*, 10.1061/(ASCE)0733-9429(2005)131:10(853), 853–861.

Vasconcelos, J. G., Wright, S. J., and Guizani, M. (2005). "Experimental investigations on rapid filling of empty pipelines." *Rep. UMCEE-05-01*, Dept. of Civil Environmental Engineering, Univ. of Michigan, Ann Arbor, MI.

Wiggert, D. C. (1972). "Transient flow in free-surface, pressurized systems." *J. Hydraul. Div.*, 98(HY1), 11–27.

Wiggert, D. C., and Tijsseling, A. S. (2001). "Fluid transients and fluid-structure interaction in flexible liquid-filled piping." *Appl. Mech. Rev.*, 54(5), 455–481.

Yamamoto, K., Arai, K., and Asamizu, T. (2000). "Transient analysis for mixed free-surface-pressure flows: Estimation of entrapped air by lumped parameter model." *Turbomachinery*, 28(6), 364–371 (in Japanese).

Zhou, F. (2000). "Effects of trapped air on flow transients in rapidly filling sewers." Ph.D. thesis, Univ. of Alberta, Edmonton, AB, Canada.

Zhou, F., Hicks, F. E., and Steffler, P. M. (2002). "Observations of air-water interaction in a rapidly filling horizontal pipe." *J. Hydraul. Eng.*, 10.1061/(ASCE)0733-9429(2002)128:6(635), 635–639.

Zhou, L., Liu, D. Y., and Karney, B. (2013a). "Investigation of hydraulic transients of two entrapped air pockets in a water pipeline." *J. Hydraul. Eng.*, 10.1061/(ASCE)HY.1943-7900.0000750, 949–959.

Zhou, L., Liu, D. Y., Karney, B., and Wang, P. (2013b). "The phenomenon of white mist in water rapidly filling pipeline with entrapped air pocket." *J. Hydraul. Eng.*, 10.1061/(ASCE)HY.1943-7900.0000765, 1041–1051.

Zhou, L., Liu, D. Y., Karney, B., and Zhang, Q. (2011). "Influence of entrapped air pockets on hydraulic transients in water pipelines." *J. Hydraul. Eng.*, 10.1061/(ASCE)HY.1943-7900.0000460, 1686–1692.